**Title:** Systematic variation in observing altitude of enhanced ion line by the pump near fifth gyroharmonic

**Authors:**

(1) Jun Wu (吴军)[1], (email: wujun1969@163.com)

(2) Jian Wu (吴健)[1],

(3) M. T. Rietveld[2,4] ,

(4) I.Haggstrom[3] ,

(5) Haisheng Zhao (赵海生)[1]

(6) Tong Xu (徐彤)[1]

(7)Zhengwen Xu (许正文)[1]

[1]National Key laboratory of electromagnetic environment, China research institute of radio wave propagation, Beijing, 102206, China

[2]EISCAT Scientific Association, 9027 Ramfjordbotn, Norway

[3]EISCAT Scientific Association, SE-981 92 Kiruna, Sweden

**E-mail:** wujun1969@163.com

**Phone:** +861080712642

**Fax number:** +861080720223

# Systematic variation in observing altitude of enhanced ion line by the pump near fifth gyroharmonic

Jun WU (吴军)[1], Jian WU (吴健)[1], M. T. RIETVELD[2] , I. HAGGSTROM[3] ,
Haisheng ZHAO (赵海生)[1] , Tong XU (徐彤)[1], Zhengwen XU (许正文)[1]

[1]National Key Laboratory of Electromagnetic Environment, China Research Institute of Radio Wave Propagation, Beijing 102206, China

[2]EISCAT Scientific Association , 9027 Ramfjordbotn, Norway

[3]EISCAT Scientific Association, SE-981 92 Kiruna, Sweden

**Abstract**

The observation of ultra high frequency (UHF) radar during an ionospheric experiment carrying out at the European Incoherent Scatter Scientific Association (EISCAT), demonstrates a systematic variation in the altitude of the pump enhanced ion line, which is quite remarkably dependent on the pump frequency, that is, when the pump frequency sweeps above the fifth gyroharmonic, the altitude of the enhanced ion line is ~ 3 km −~ 6 km lower than that at the pump frequency very close to the fifth gyroharmonic. The analysis shows that the systematic variation in the altitude of the pump enhanced ion line is principally dependent on the enhanced electron temperature, although the changes in the profile of the electron density brought about by the ionospheric heating are not independent of those systematic altitude variations.

**Keywords**：ionospheric heating, enhance ion line, UHF radar, observing altitude, Bragg condition

(Some figures may appear in colour only in the online journal)

## 1. Introduction

Only the temperature and density modifications were originally intended in the early ionospheric heating experiments, but a much greater variety of physical phenomena have been observed, among which one of the most interesting is the parametric instability, which has been extensively studied [1-18].

During an ionospheric heating experiment, the enhanced plasma line and ion line observed by Incoherent Scattering radar (ISR) provide the signatures of parametric decay instability (PDI) and oscillation two stream instability (OTSI), where plasma line and ion line are the ISR spectrum scattered from the high frequency electrostatic Langmuir wave and the low frequency ion acoustic wave, respectively, by which such plasma parameters as electron density, electron temperature, ion temperature and ion drift velocity can be obtained. Based on those observations, the structure of the ISR spectrum [8, 11, 12, 19-25], the threshold to excite PDI and OTSI [10，26-28], the characteristic time of PDI and OTSI [12, 20, 21, 25, 29, 30] and the altitude characteristic of the enhanced plasma line and ion line [11, 12, 31-34] have been investigated. Previously, considering the ionosphere as a doubly refracting medium with the presence of the magnetic field, PDI and OTSI was expected to be excited only by O mode pump [21, 29]. However, Blagoveshchenskaya *et al* [35] found that the X mode pump could also excite the enhanced down-shifted and up-shifted ion lines and down-shifted plasma line.

Usually, the pump enhanced Langmuir and ion acoustic waves are induced by PDI and OTSI in an altitude range extending from the reflection altitude of the pump downward to altitudes where resonant Langmuir waves having large wave numbers are heavily Landau damped [11]. The width of excitation range is $0.1H$, where $H$ is the scale height of ionosphere [11]. The enhanced Langmuir and ion acoustic waves travel downward and should be observed by radar at an altitude where the Bragg condition of radar can be satisfied [11, 12, 36]. Djuth *et al* [31] presented some observations at the European Incoherent Scatter Scientific Association (EISCAT) that the observed plasma turbulence excited by the pump at 6.77 MHz plunged downward in altitude over timescales of tens of seconds after the pump on, and claimed that this phenomenon was most likely caused by the change in the electron density profile brought about by the ionospheric heating. The EISCAT ultra high frequency (UHF) radar observed a persistent enhancement in ion line induced by an O mode pump at frequency 5.423 MHz, which started at ~ 230 km and descended to ~ 220 km within ~ 60 s in the heating period [32]. Ashrafi *et al* [32] claimed that the clear descent in the altitude of the enhanced ion line represented the change in the profile of electron density.

By considering a constant ionospheric scale height of ~ 50 km, Wu *et al* [33] studied those altitude variations in the enhanced ion and plasma lines observed during an ionospheric heating experiment carried out on 11 Mar. 2014 at EISCAT Tromsø site, and suggested that those altitude variations are due to the enhancement in electron temperature and the change in the profile of electron density. However, they didn't clearly identify the dominant one of the above two mechanisms. In this paper, considering the ionospheric scale height as a function of plasma temperature, the observing altitude of the enhanced ion line excited by an O mode pump near fifth electron gyroharmonic is studied in more detail, and the dominant mechanism leading to those altitude variations in the enhanced ion line is identified.

## 2. Experiment and data

The ionospheric heating experiment reported here was carried out at 12:30UT −14:30UT (Universal Time) on 11 Mar. 2014 at EISCAT site near Tromsø in northern Norway (69.58° N, 19.21° E, magnetic dip angle $I$=78°). The EISCAT heater [37, 38] transmitted with an effective radiated power (ERP) of 56 – 78 MW and O mode polarization and with a modulation cycle of 18 min on and 12 min off. The pump frequency $f_{\mathrm{HF}}$ was changed in steps of 2.804 kHz in the range of [6.7 MHz, 7 MHz] with a period of 10 s, as illustrated in the bottom panel of figures 2 and 3. The pump beam was field-aligned (12.5° zenith, 186.2° azimuth). Indeed, it is believed that when $f_{\mathrm{HF}}$ lies near the electron gyroharmonics, the anomalous absorption of the pump will be greatly reduced. This prompted an investigation into ionospheric heating at $f_{\mathrm{HF}}$ close to $5f_{\mathrm{ce}}$, where $f_{\mathrm{ce}}$ is the local electron cyclotron frequency and has a value of ~1.366 MHz at an altitude of ~ 200 km in Tromsø.

The EISCAT UHF ISR [39] started observations at 12:32:30 UT and remained field aligned with the ‘beata’ mode. The ‘beata’ mode has a $640\,\mu\mathrm{s}$ $(32\times 20\,\mu\mathrm{s})$ alternating code pulse with 10 μs sampling，which resulted in a decoded range resolution of ~ 2.5 km. In addition, to measure the effect induced by the pump for each step of frequency, the data was analyzed using an integration time of 10 s by version 8.7 of GUISDAP (Grand United Incoherent Scatter Design and Analysis

Package) software [40] and version 2.67 of RTG (Real Time Graphic), which are provided by EISCAT.

The local geomagnetic condition was relatively inactive during the experiment. Figure 1 shows the total magnetic strength on the ground and at an altitude of 200 km. The total magnetic strength on the ground, which was recorded at Tromsø Geophysical Observatory (UiT, The Arctic University of Norway), varied in the interval of **[**53452.5 nT, 53485 nT**]**, where "**[ ]**" denotes the closed interval. The total magnetic strength at an altitude of 200 km, which is obtained by extrapolating the total magnetic strength on the ground, varies in the interval of **[**49202 nT, 49233 nT**]**. Thus, the corresponding $5f_{\mathrm{ce}}$ should be in the interval of **[**6.892 MHz, 6.896 MHz**]**, which exactly lies in the interval of **[**6.7 MHz, 7 MHz**]**.

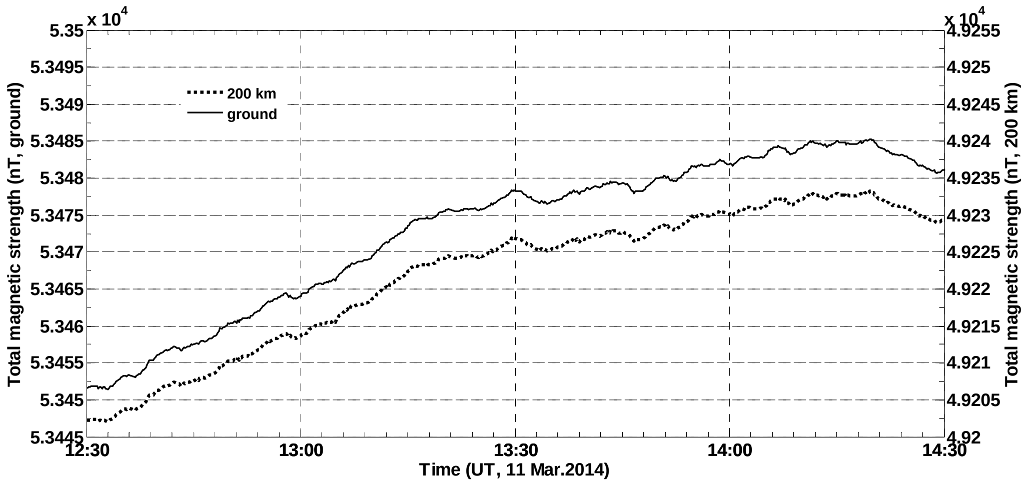


**Figure 1.** The total magnetic strength during the experiment in Tromsø, where the solid curve and dashed curve represent the values on the ground and at an altitude of 200 km, respectively.

The normalized ion lines within the band of [−20 kHz, 20 kHz] at several altitudes of 215.43 km, 212.5 km, 209.57 km, 206.63 km, 203.7 km and 200.77 km, are given in the 1st – 6th panels of figure 2, respectively. One can see that the enhanced ion lines of up to ~ 1 occur only at a particular altitude and within an particular pump frequency band, namely, at an altitude of 206.63 km and within the band of [6.871028 MHz, 6.848598 MHz] in the first heating cycle, 215.43 km and [6.826168 MHz, 6.840187 MHz] in the second heating cycle, 209.57 km and [6.857009 MHz, 6.842991 MHz] in the third heating cycle, 212.5 km and [6.834579 MHz, 6.854206 MHz] in the fourth heating cycle. On the other hand, within those pump frequency bands, some gaps or weak ion line spectra appear at other altitudes, which are caused by the normalization to the strongest value of ion line at any particular time and altitude and don't imply a real decrease in ion line or any unusual response.

When $f_{\mathrm{HF}}$ sweeps above 6.871028 MHz in the first heating cycle, above 6.840187 MHz in the second heating cycle, above 6.857009 MHz in the third heating cycle and above 6.854206 MHz in the fourth heating cycle, the enhanced ion lines are up to ~ 0.85 and occur in a lower altitude range, namely, at the altitudes of 203.7 km and 200.77 km in the first heating cycle, 212.5 km and 209.57 km in the second heating cycle, 209.57 km and 206.63 km in the third and fourth heating cycle. Those remarkable extensions of observing altitude of the enhanced ion line are due to the dependence of the wave number of the traveling ion acoustic wave on the profiles of enhanced electron temperature and ion mass [34]. When $f_{\mathrm{HF}}$ is below 6.848598 MHz in the first heating cycle, below 6.826168 MHz in the second heating cycle, below 6.842991 MHz in the third heating cycle and below 6.834579 MHz in the fourth heating cycle, however, no enhanced ion lines are found, for which the mechanism being responsible is beyond the scope of this paper.

In order to facilitate the following descriptions and discussions, a convention of the division of $f_{\mathrm{HF}}$ is adopted: the pump frequency band of [6.7 MHz, 7 MHz] will be divided into three bands according to the systematic variation in the intensity of ion line, namely, the higher band (HB, above $5f_{\mathrm{ce}}$), the gyroharmonic band (GB, very close to $5f_{\mathrm{ce}}$) and the lower band (LB, below $5f_{\mathrm{ce}}$). For instance, we choose the HB to be **(**6.857009 MHz, 7 MHz**]**, the GB to be **[**6.84299 MHz, 6.857009 MHz**]** and the LB to be **[**6.7 MHz, 6.84299 MHz**)** in the third heating cycle, where "**( )**" means the open interval. Due to the variation of the geomagnetic field indicated in figure 1, however, the above division in each heating cycle should be slightly different from each other. Indeed, the GB is the band of **[**6.871028, 6.848598**]** in the first heating cycle, the band of **[**6.826168, 6.840187**]** in the second heating cycle, the band of **[**6.857009, 6.842999**]** in the third heating cycle, and the band of **[**6.834579, 6.854206**]** in the fourth heating cycle.

Two prominent features of the enhanced ion line shared in the HB and GB are the significant "spike" in the center of the ion line spectra, which is the manifestation of the oscillating two stream instability (OTSI) or the purely growing instability, and the significant "shoulder" lying at frequency ~ 9.45 kHz, which is the confirmation of the parametric decay instability (PDI) [11, 12].

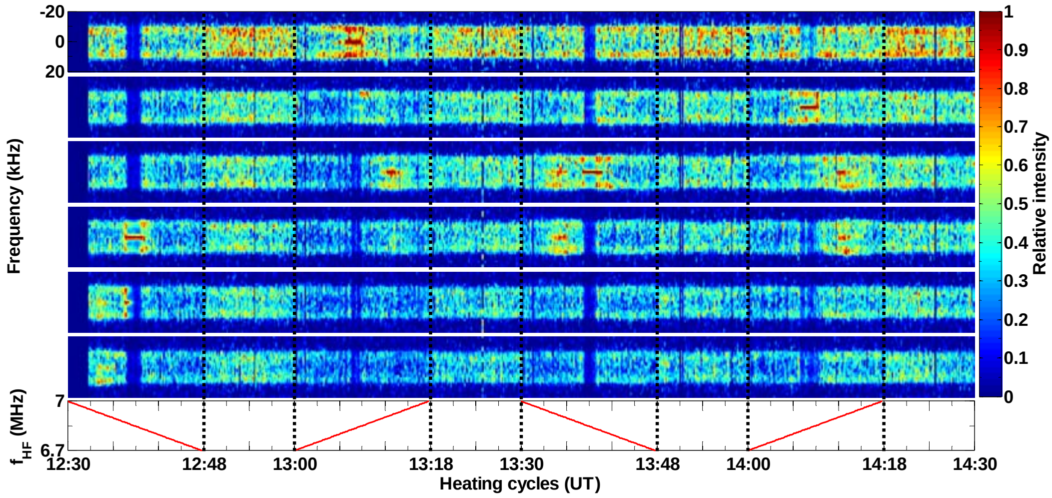


**Figure 2.** The ion line at several altitudes of 215.43 km (1st panel), 212.5 km (2nd panel), 209.57 km (3rd panel), 206.63 km (4th panel), 203.7 km (5th panel) and 200.77 km (6th panel) versus heating cycles (7th panel).

Figure 3 gives the altitude profile of electron temperature $T_e$ with the height resolution of 13 – 19 km. Near an altitude of 200 km, it is evident that the enhanced $T_e$ is a function of $f_{HF}$, that is, $T_{eLB200} > T_{eHB200} > T_{eGB200}$, where $T_{eLB200}$, $T_{eHB200}$ and $T_{eGB200}$ are the electron temperature in the LB, HB and GB at an altitude of ~ 200 km, respectively. The means of $T_{eLB200}$, $T_{eHB200}$ and $T_{eGB200}$ are $\sim 2782$ K, $\sim 2687$ K and $\sim 2268$ K in the first heating cycle, $\sim 2882$ K, $\sim 2505$ K and $\sim 2103$ K in the second heating cycle, $\sim 2815$ K, $\sim 2581$ K and $\sim 2348$ K in the third heating cycle, $\sim 2667$ K, $\sim 2599$ K and $\sim 2186$ K in the fourth heating cycle, respectively. This variation in $T_e$ with $f_{HF}$ is dependent on the dispersion behavior of the electrostatic upper hybrid wave excited by an O mode pump lying in the GB, HB and LB respectively [41, 42]. In general, the upper hybrid resonance altitude of the pump is about 2 − 10 km lower than the reflection altitude of the pump, which is dependent on the altitude profile of ionospheric electron density [43].

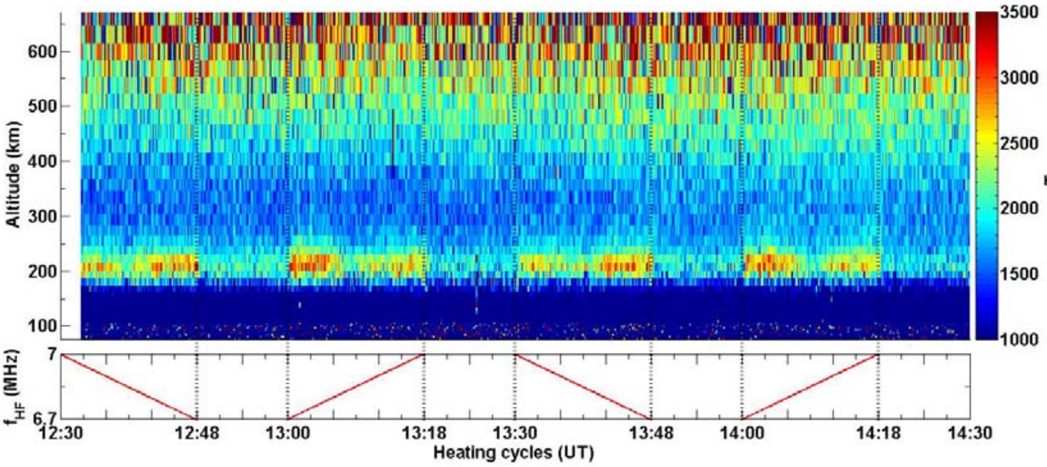


**Figure 3.** The electron temperature $T_e$ versus heating cycles.

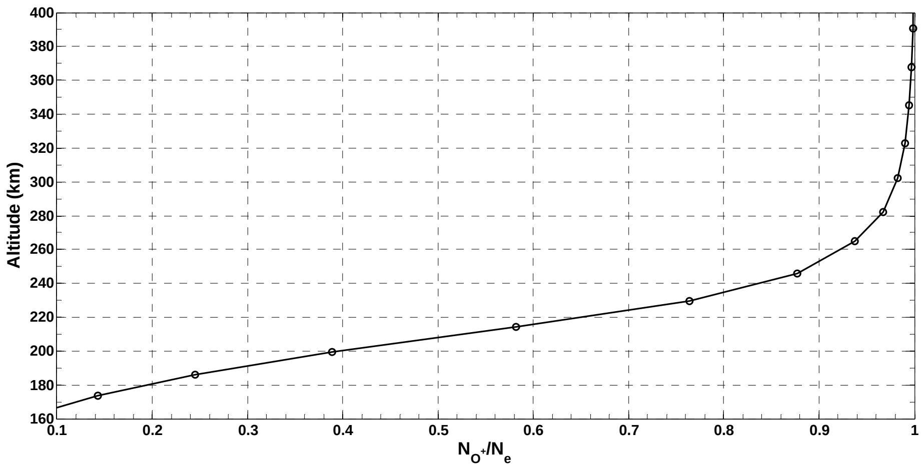


**Figure 4.** The ratio of $N_{O^+}$ to $N_e$ as an altitude function.

Figure 4 illustrates the ratio of oxygen ion density $N_{O^+}$ to electron density $N_e$ as a function of altitude, which is given by International Reference Ionosphere 2007 (IRI-2007) model [44]. Obviously, $\frac{N_{O^+}}{N_e}$ monotonically descends with the descending in altitude, and the gradient of $\frac{N_{O^+}}{N_e}$ becomes steeper in the altitude range of 170−260 km. This imply that $\frac{N_{O_2^+}}{N_e}$ and $\frac{N_{NO^+}}{N_e}$ monotonically increase with the descending in altitude, where $N_{O_2^+}$ and $N_{NO^+}$ are the molecular oxygen ion density and nitric oxide ion density, respectively. Notably, for the sake of simplicity, only $O^+$, $O_2^+$ and $NO^+$ will be considered in this study, whereas hydrogen ion $H^+$, atomic nitrogen ion $N^+$ and helium ion $H_e^+$ are ignored due to the small mass or the small percentage.

## 3. Discussion

To avoid excessive Landau damping, the enhanced Langmuir and ion acoustic waves are excited by PDI and OTSI in the altitude interval of [11]

$$h_0 - 0.1H \le h_{ex} < h_0 \tag{1}$$

where $h_{ex}$ is the exciting altitude of PDI and OTSI, $h_0$ the reflection altitude of the pump and $H$ the scale height of ionosphere. Considering that $H$ is ~ 30 km – ~ 40 km for typical ionosphere [31], it can be reasonably assumed that the reflection altitudes of the pump in the GB are approximately identical to that in the HB, namely, $h_{0HB} \approx h_{0GB}$, where $h_{0HB}$ and $h_{0GB}$ indicate the reflection altitudes of the pump in the HB and GB, respectively. This assumption is supported by those ionograms measured by the Dynasonde HF sounder at EISCAT during the experiment, which show that the reflection altitudes of the pump at 6.7 MHz, 6.85 MHz and 7 MHz are ~ 213.7 km, ~ 215.7 km and ~ 217.8 km, respectively.

The enhanced ion acoustic and Langmuir waves can travel downward and be observed by a radar in monostatic operation at the altitude [11]

$$h = h_0 - \Delta h \tag{2}$$

where $\Delta h = 12 \dfrac{K_B f_r^2}{m_e c^2 f_{HF}^2} T_e H$ , $K_B$ denotes the Boltzmann constant, $f_r$ radar frequency, $m_{\mathrm{e}}$ the electron mass, and c the velocity of light. Obviously, $\Delta h$ is dependent on $T_{\mathrm{e}}$ and $H$ of plasma on the traveling path.

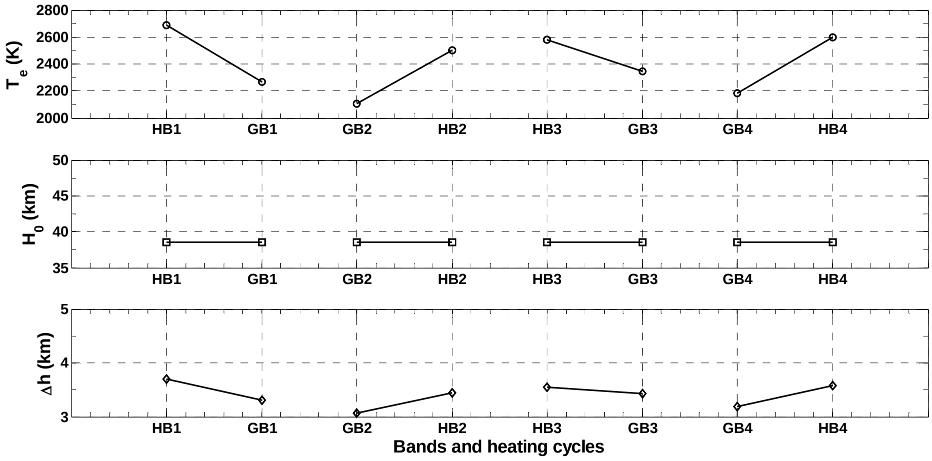


**Figure 5.** $T_{\mathrm{e200km}}$, $H_0$ and $\Delta h$ during the experiment, where $T_{\mathrm{e200km}}$ is the mean of electron temperature around an altitude of 200 km, $H_0$ is the scale height of background ionosphere. The tick labels of abscissa denote the pump frequency bands and the heating cycles, e.g. HB1 for the HB in the first heating cycle.

The scale height $H$ can be defined as [45]

$$\frac{1}{H} = -\frac{1}{N_{\mathrm{e}}}\frac{\mathrm{d}N_{\mathrm{e}}}{\mathrm{d}h} = \frac{m_{\mathrm{i}} g}{\mathrm{K_B} T_{\mathrm{p}}} + \frac{m_{\mathrm{i}} \nu_{\mathrm{in}} W_{\mathrm{D}}}{K_{\mathrm{B}} T_{\mathrm{p}}} + \frac{\mathrm{d}T_{\mathrm{p}} / \mathrm{d}h}{T_{\mathrm{p}}} \tag{3}$$

where $m_{\mathrm{i}}$ is the ion mass, $g$ the acceleration due to gravity, $T_{\mathrm{p}} = \dfrac{T_{\mathrm{i}} + T_{\mathrm{e}}}{2}$ the plasma temperature, $\nu_{\mathrm{in}}$ the collision frequency of ion with neutrals and $W_{\mathrm{D}}$ the diffusion velocity of ions. Considering atomic oxygen as the most common ion species at the F2 region and using $m_{\mathrm{i}} \approx 2.657 \times 10^{-26}$ kg, $\nu_{\mathrm{in}} \approx 4.1$ Hz for the typical ionosphere [46] and $W_{\mathrm{D}} \approx 3.7$ m/s [40, 41], $T_{\mathrm{p}} \approx 1900$ K obtained at 14:28:00 UT – 14:30:00 UT, $H_0$ for the background ionosphere has a value of ~ 38.6 km and is shown in the 2nd panel of figure 5. It can be seen that the higher $T_{\mathrm{e200km}}$ tends to increase $\Delta h$ in the GB and HB during the experiment, as expected by formula (2).

When the pump lies in the GB, the UHF radar can observe the enhanced ion lines at $h_{\mathrm{GB1}} = h_0 - 3.3$ km , $h_{\mathrm{GB2}} = h_0 - 3.1$ km , $h_{\mathrm{GB3}} = h_0 - 3.4$ km and $h_{\mathrm{GB4}} = h_0 - 3.2$ km in the first, second, third and fourth heating cycles, respectively. In the HB, the UHF radar observing altitudes are $h_{\mathrm{HB2}} = h_0 - 3.4$ km , $h_{\mathrm{HB3}} = h_0 - 3.6$ km and $h_{\mathrm{HB4}} = h_0 - 3.6$ km in the first, second, third and fourth heating cycles, respectively. In addition, $h_{\mathrm{GB1}} - h_{\mathrm{HB1}} = 0.4$ km , $h_{\mathrm{GB2}} - h_{\mathrm{HB2}} = 0.2$ km , $h_{\mathrm{GB3}} - h_{\mathrm{HB3}} = -0.2$ km and $h_{\mathrm{GB4}} - h_{\mathrm{HB4}} = 0.4$ km . Obviously, considering the altitude ambiguity in the measurement of UHF radar, the distributing trend of the observing altitude shown in the 3rd panel of figure 5 is in agreement with that shown in figure 2. In addition, it is necessary to point out that formulas (1) and (2) were obtained based on the description of the ionospheric electron density profile $N_{\mathrm{e}}(h) = N_{\mathrm{e}}(h_0)\left(1 + \dfrac{h - h_0}{H}\right)$ rather than the typical or real ionospheric electron density profile [11].

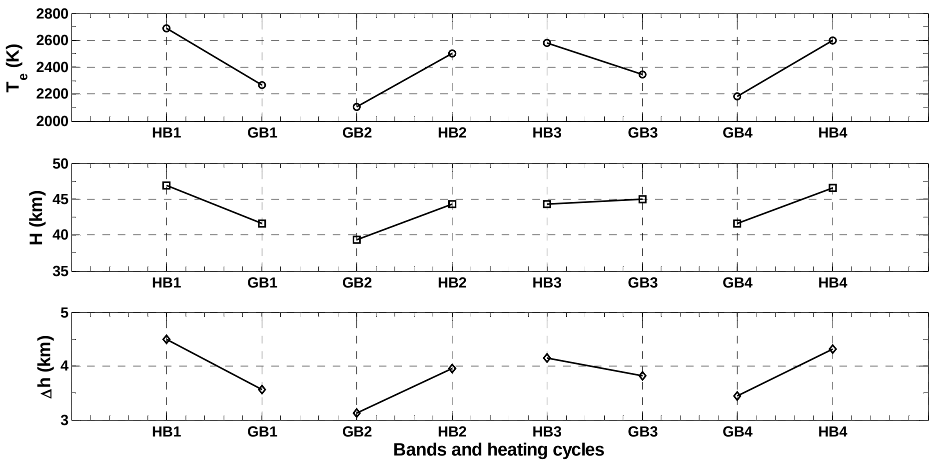


**Figure 6.** The same as figure 5 but for $H$ , where $H$ is the real time scale height of ionosphere during the ionospheric heating.

Indeed, formula (3) describes that the real time $H$ is essentially dependent on the electron density profile of ionosphere under the controls of gravity, diffusion and temperature gradient. Thus, $H$ during the experiment are available and have values of 46.85 km in the HB and 41.65 km in the GB in the first heating cycle, 44.33 km and 39.38 km in the second heating cycle, 44.33 km and 45.01 km in the third heating cycle and 46.6 km and 41.63 km in the fourth heating cycle, as shown in the 2nd panel of figure 6. One can see that the higher $T_{\mathrm{e200km}}$ tends to increase $H$ in the first, second and fourth heating cycles, implying that the first and second terms in the right side of formula (3) play the dominant role in $H$. This is because the higher electron temperature can make electron overcome more effectively the gravity as well as the collisions and further escape from the heated region, slightly reshaping the local altitude profile of the ionosphere. In the third heating cycle, however, $H$ in the GB is somewhat larger than that in the HB. This may be due to the temperature gradient in the GB as shown in figure 3 and the 1st panel of figure 6. It is shown that the third term in the right side of formula (3) may play an important role in $H$ in the third heating cycle.

The 3rd panel of figure 6 illustrates $\Delta h$ in the GB and HB during the experiment. When the pump lies in the GB, the UHF radar can observe the enhanced ion lines at several altitudes of $h_{\mathrm{GB1}} = h_0 - 3.56$ km, $h_{\mathrm{GB2}} = h_0 - 3.13$ km, $h_{\mathrm{GB3}} = h_0 - 3.82$ km and $h_{\mathrm{GB4}} = h_0 - 3.44$ km in the first, second, third and fourth heating cycles, respectively. In the HB, the UHF radar observing altitudes are $h_{\mathrm{HB1}} = h_0 - 4.49$ km, $h_{\mathrm{HB2}} = h_0 - 3.96$ km, $h_{\mathrm{HB3}} = h_0 - 4.15$ km and $h_{\mathrm{HB4}} = h_0 - 4.32$ km in the first, second, third and fourth heating cycles, respectively. Furthermore, one can find $h_{\mathrm{GB1}} - h_{\mathrm{HB1}} = 0.93$ km, $h_{\mathrm{GB2}} - h_{\mathrm{HB2}} = 0.82$ km,

$h_{\mathrm{GB3}} - h_{\mathrm{HB3}} = -0.33\ \mathrm{km}$ and $h_{\mathrm{GB4}} - h_{\mathrm{HB4}} = 0.88\ \mathrm{km}$. Especially, it should be noted that $h_{\mathrm{GB3}} - h_{\mathrm{HB3}} = -0.33\ \mathrm{km}$ is small enough so that the enhanced ion lines both in the GB and HB in the third heating cycle may lie in the same range gate of the radar and are observed at the altitude of 209.57 km as shown in figure 2. Obviously, the distribution of the observing altitude shown in the 3rd panel of figure 5 is in perfect agreement with that shown in figure 2.

Even so, the comparison between figure 5 and figure 6 shows that the distributing trend of the observing altitude has not been changed by the change in the scale height of ionosphere, that is, the distributing trend of the observing altitude is essentially dependent on $T_{\mathrm{e}}$ and is rather less on $H$.

The dependence of the observing altitude of the enhanced ion line on $T_{\mathrm{e}}$ can be described by the dispersion relation of ion acoustic wave. With regard to the field aligned observation of radar in monostatic operation, the ion acoustic wave traveling in a non-uniform but stationary ionosphere will follow the dispersion function [12]

$$\omega_{\mathrm{ia}}^2 = \gamma \frac{\mathrm{K_B} T_{\mathrm{e}}}{m_{\mathrm{i}}} k_{\mathrm{ia}}^2 \tag{4}$$

where $\gamma$ is the adiabatic index, $m_{\mathrm{i}}$ the effective ion mass, and $k_{\mathrm{ia}}$ the wave number of ion acoustic wave respectively. When the ion acoustic wave travel down in ionosphere, $\omega_{\mathrm{ia}}$ will not change, whereas $k_{\mathrm{ia}}$ may change. When $k_{\mathrm{ia}} = 2k_{\mathrm{r}}$, namely, ion acoustic wave satisfies the Bragg condition, the enhanced ion acoustic wave will be observed, where $k_{\mathrm{r}}$ is the wave number of radar. Thus, assuming $T_{\mathrm{e}} = T_{\mathrm{e}}'$, the ion acoustic wave can be observed at an altitude $h'$, where $2k_{\mathrm{r}} = \sqrt{\frac{\omega_{\mathrm{ia}}^2}{\gamma \mathrm{K_B}} \frac{m_{\mathrm{i}}'}{T_{\mathrm{e}}'}}$. On the other hand, if $T_\mathrm{e} = T_\mathrm{e}'' > T_\mathrm{e}'$ is assumed, then the ion acoustic wave can be observed at other altitude $h''$, where $2k_\mathrm{r} = \sqrt{\frac{\omega_\mathrm{ia}^2}{\gamma \mathrm{K_B}} \frac{m_\mathrm{i}''}{T_\mathrm{e}''}}$. Thus $\frac{m_\mathrm{i}''}{T_\mathrm{e}''} = \frac{m_\mathrm{i}'}{T_\mathrm{e}'}$ and $m_\mathrm{i}'' > m_\mathrm{i}'$ can be obtained. Due to the monotonicity of the profile of the effective ion mass, then $h''$ will be lower than $h'$.

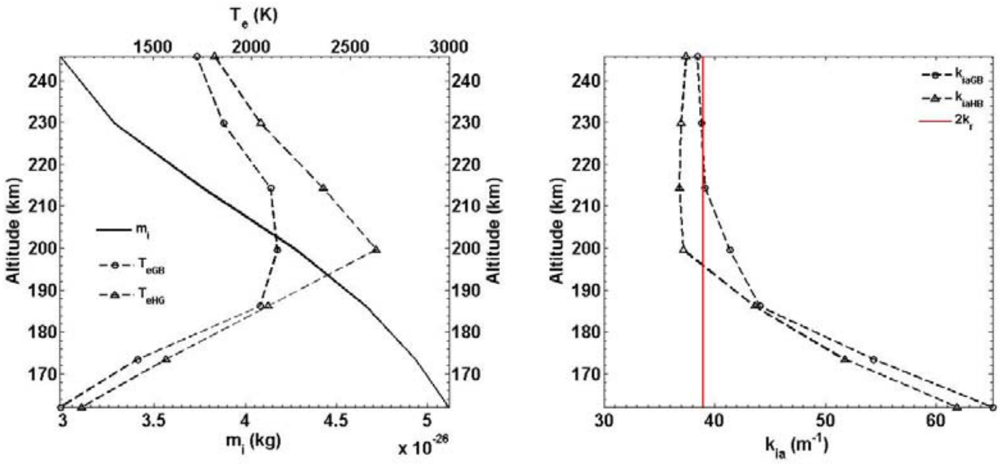


**Figure 7.** The profiles of $m_\mathrm{i}$, $T_\mathrm{eGB}$, $T_\mathrm{eHB}$ (the left panel), $k_\mathrm{iaGB}$ and $k_\mathrm{iaHB}$ (the right panel) within an altitude range of 162.1 − 245.8 km in the fourth heating cycle.

As an example, the enhanced ion line in the fourth heating cycle is examined. The left panel of figure 7 gives the respective profiles of $m_\mathrm{i}$, $T_\mathrm{eGB}$ and $T_\mathrm{eHB}$, demonstrating that $m_\mathrm{i}$, $T_\mathrm{eGB}$ and $T_\mathrm{eHB}$ become larger with the descent in altitude above altitude ~ 199.6 km. Here, the effective ion mass $m_\mathrm{i} = \frac{N_{\mathrm{O}^+}}{N_\mathrm{e}} m_{\mathrm{io}^+} + \left(1 - \frac{N_{\mathrm{O}^+}}{N_\mathrm{e}}\right) m_{\mathrm{io}_2^+}$, where $\frac{N_{\mathrm{O}^+}}{N_\mathrm{e}}$ is obtained from figure 4. $m_{\mathrm{io}^+} = 2.657 \times 10^{-26}$ kg and $m_{\mathrm{io}_2^+} = 5.314 \times 10^{-26}$ kg. Due to $m_{\mathrm{iO}_2^+} \approx m_{\mathrm{iNO}^+}$, $\mathrm{O}_2^+$ and $\mathrm{NO}^+$ are considered in the combining way. $T_\mathrm{eGB}$ is the mean of electron temperature within the internal of [14:07:20 UT, 14:09:10 UT], and $T_\mathrm{eHB}$ is the mean of electron temperature within the internal of [14:11:20 UT, 14:18:00 UT]. The right panel of figure 7 indicates that $k_{\mathrm{iaGB}} = 2k_{\mathrm{r}}$ at altitude $h_{\mathrm{GB}} =\sim 222\ \mathrm{km}$, whereas $k_{\mathrm{iaHB}} = 2k_{\mathrm{r}}$ at altitude $h_{\mathrm{HB}} =\sim 196\ \mathrm{km}$, where $k_{\mathrm{r}} = 19.5\ \mathrm{m}^{-1}$ for EISCAT UHF radar, $k_{\mathrm{iaGB}}$ and $k_{\mathrm{iaHB}}$ are the wave numbers of the enhanced ion acoustic wave in the GB and HB, respectively.

With the comparison between figure 2 and the right panel of figure 7, however, some errors of the altitude are obvious. That is, $Dh = 26\ \mathrm{km}$ in the right panel of figure 7, whereas $Dh = 2.9\ \mathrm{km}$ in figure 2, where $Dh = h_{\mathrm{GB}} - h_{\mathrm{HB}}$. Those errors may be in two aspects, namely, the uncertainty in the altitude profile of the effective ion mass $m_{\mathrm{i}}$ and the ambiguity in the altitude profile of electron temperature $T_{\mathrm{e}}$. Indeed, considering a small $\frac{\mathrm{d}T_{\mathrm{e}}}{\mathrm{d}h}$, the larger $\frac{\mathrm{d}m_{\mathrm{i}}}{\mathrm{d}h}$ will compress $Dh$, where $\frac{\mathrm{d}T_{\mathrm{e}}}{\mathrm{d}h}$ and $\frac{\mathrm{d}m_{\mathrm{i}}}{\mathrm{d}h}$ are the gradients of the altitude profile of $T_{\mathrm{e}}$ and $m_{\mathrm{i}}$, respectively. On the other hand, if a small $\frac{\mathrm{d}m_{\mathrm{i}}}{\mathrm{d}h}$ is considered, then the larger $\frac{\mathrm{d}T_{\mathrm{e}}}{\mathrm{d}h}$ will also compress $Dh$.

## 4. Conclusions

This paper focuses on the observing altitude of the enhanced ion line during an ionospheric heating experiment with a pump frequency near the fifth electron gyroharmonic on 11 Mar. 2014 at EISCAT Tromsø site in northern Norway.

Those UHF observations show that the observing altitude of the enhanced ion line varies as a function of pump frequency. When the pump frequency lies above the fifth electron gyroharmonic, the electron temperature near upper hybrid resonance altitude of the pump is ~ 400 K higher than that at the pump frequency very close to the fifth gyroharmonic, and the altitude of the enhanced ion line is ~ 3 km −~ 6 km lower than that at the pump frequency very close to the fifth gyroharmonic.

The analysis shows that when the pump frequency lies above the fifth electron gyroharmonic, the descent of altitude of the enhanced ion line is principally brought about by the modification of the electron temperature near upper hybrid resonance altitude, whereas the modification of the electron density profile by the ionospheric heating also contributes to the descent of altitude of the enhanced ion line, but it is not dominant.


## Acknowledgments

We would like to thank the engineers of EISCAT in Tromsø for keeping the facility in excellent working condition, and Tromsø Geophysical Observatory, UiT The Arctic University of Norway, for providing the magnetic data in Tromsø recorded on 11 Mar. 2014. The data of UHF radar can be freely obtained from EISCAT (http://www.eiscat.se/schedule/schedule.cgi). The EISCAT Scientific Association is supported by China (China Research Institute of Radiowave Propagation), Finland (Suomen Akatemia of Finland), Japan (the National Institute of Polar Research of Japan and Institute for Space-Earth Environmental Research at Nagoya University), Norway (Norges Forkningsrad of Norway), Sweden (the Swedish Research Council) and the UK (the Natural Environment Research Council).


## References


[1] Silin V P 1965 *Sov. Phys. JETP* **21** 1127

[2] DuBois D F and Goldman M V 1965 *Phys. Rev. Lett.* **14** 544

[3] DuBois D F and Goldman M V 1967 *Phys. Rev.* **164** 207

[4] Perkins F W and Flick J 1971 *Phys. Fluids* **14** 2012

[5] Rosenbluth M N 1972 *Phys*. *Rev*. *Lett*. **29** 565

[6] Drake J F *et al* 1974 *Phys*. *Fluids* **17** 778

[7] Perkins F W, Oberman C and Valeo E J 1974 *J*. *Geophys*. *Res*. **79** 1478

[8] Kuo Y Y and Fejer J A 1972 *Phys*. *Rev*. *Lett*. **29** 1667

[9] Kuo S P and Cheo B R 1978 *Phys*. *Fluids* **21** 1753

[10] Fejer J A 1979 *Rev*. *Geophys*. **17** 135

[11] Stubbe P, Kohl H and Rietveld M T 1992 *J*. *Geophys*. *Res*. **97** 6285

[12] Kohl H *et al* 1993 *J*. *Atmos*. *Terr*. *Phys*. **55** 601

[13] Wu J, Wu J and Xue Y R 2006 *Int*. *J*. *Comput*. *Fluid Dyn*. **20** 491

[14] Wu J, Wu J and La Hoz C 2007 *Chin*. *Phys*. **16** 558

[15] Gao X L *et al* 2013 *Phys*. *Plasmas* **20** 072902

[16] Gao X L *et al* 2014 *Astrophys*. *J*. **780** 56

[17] He P *et al* 2016 *Astrophys*. *J*. **827** 64

[18] Ke Y G *et al* 2017 *Phys*. *Plasmas* **24** 012108

[19] Carlson H C, Gordon W E and Showen R L 1972 *J*. *Geophys*. *Res*. **77** 1242

[20] Gordon W E and Carlson H C Jr 1974 *Radio Sci*. **9** 1041

[21] Kantor I J 1974 *J*. *Geophys*. *Res*. **79** 199

[22] Hagfors T *et al* 1983 *Radio Sci*. **18** 861

[23] DuBois D F, Rose H A and Russell D 1988 *Phys*. *Rev*. *Lett*. **61** 2209

[24] Nordling J A *et al* 1988 *Radio Sci*. **23** 809

[25] Stubbe P *et al* 1985 *J*. *Atmos*. *Terr*. *Phys*. **47** 1151

[26] Bezzerides B and Weinstock J 1972 *Phys*. *Rev*. *Lett*. **28** 481

[27] Weinstock J and Bezzerides B 1972 *J. Geophys. Res.* **77** 761

[28] DuBois D F and Goldman M V 1972 *Phys. Fluids* **15** 919

[29] Carlson H C, Gordon W E and Showen R L 1972 *J. Geophys. Res.* **77** 1242

[30] Jones T B *et al* 1986 *J. Atmos. Terr. Phys.* **48** 1027

[31] Djuth F T *et al* 1994 *J. Geophys. Res.* **99** 333

[32] Ashrafi M, Kosch M J and Honary F 2006 *Adv. Space Res.* **38** 2645

[33] Wu J *et al* 2017 *Plasma Sci. Technol.* **19** 125303

[34] Wu J *et al* 2018 *J. Geophys. Res.* **123** 918

[35] Blagoveshchenskaya N F *et al* 2014 *J. Geophys. Res.* **119** 10483

[36] Kohl H *et al* 1987 *Radio Sci.* **22** 655

[37] Rietveld M T *et al* 1993 *J. Atmos. Terr. Phys.* **55** 577

[38] Rietveld M T *et al* 2016 *Radio Sci.* **51** 1533

[39] Rishbeth H and Van Eyken A P 1993 *J. Atmos. Terr. Phys.* **55** 525

[40] Lehtinen M S and Huuskonen A 1996 *J. Atmos. Terr. Phys.* **58** 435

[41] Wu J, Wu J and Xu Z W 2016 *Plasma Sci. Technol.* **18** 890

[42] Wu J *et al* 2017 *J. Geophys. Res.* **122** 1277

[43] Gurevich A V 2007 *Phys. Usp.* **50** 1091

[44] Bilitza D and Reinisch B W 2008 *Adv. Space Res.* **42** 599

[45] Liu L B *et al* 2007 *J. Geophys. Res.* **112** A06307

[46] Rishbeth H and Garriott O K 1969 *Introduction to Ionospheric Physics* (New York: Academic Press)